

# Self-mixing instrument for simultaneous distance and speed measurement

Michele Norgia \*, Dario Melchionni, Alessandro Pesatori

*Dipartimento di Elettronica, Informazione e Bioingegneria Politecnico di Milano, Via Ponzio 34/5, Milano, Italy*

A novel instrument based on Self-mixing interferometry is proposed to simultaneously measure absolute distance and velocity. The measurement method is designed for working directly on each kind of surface, in industrial environment, overcoming also problems due to speckle pattern effect. The laser pump current is modulated at quite high frequency (40 kHz) and the estimation of the induced fringes frequency allows an almost instantaneous measurement (measurement time equal to 25  $\mu$ s). A real time digital elaboration processes the measurement data and discards unreliable measurements. The simultaneous measurement reaches a relative standard deviation of about  $4 \cdot 10^{-4}$  in absolute distance, and  $5 \cdot 10^{-3}$  in velocity measurement. Three different laser sources are tested and compared. The instrument shows good performances also in harsh environment, for example measuring the movement of an opaque iron tube rotating under a running water flow.

**Keywords:** Interferometry, Self-mixing, Velocity measurement, Distance measurement, Laser sensors, Laser doppler

## 1. Introduction

A strong interest in contactless distance and speed measurements is growing in many fields, like in fabrication processes, quality tests and consumer electronic industry. Several optic techniques are able to monitor displacement and speed [1], but normally not simultaneously. Each technique is optimized for different application area, depending on range and resolution required. Triangulation and time of flight are the most widespread and extensive applied. The first one is suitable in the near range (up to 10 m), and the second one, on the contrary, for long distances (kilometers), but with limited resolution (from some millimeters to a few centimeters). Both of them show a clear trade-off between resolution and maximum distance. Coherent telemeter, although, can reach a better resolution, down to the micrometer scale [2], and a range wider than triangulation telemeter, but with a huge drawback: setup complexity and cost. However, two optical channel fabrication and calibration problem has been recently overcome by Self-mixing- Interferometry [3,4]. This technique is based on laser Doppler effect, directly acting on the laser diode emission. It is time-saving and user-friendly at the same time, while keeping the properties of laser Doppler interferometric techniques. All these features, which are deeply described in the literature [5–13], were used to design new measurement instruments, also for industrial applications [14–19]. Furthermore, new electronic technologies allow implementing novel real-time algorithms, able to process the self-mixing signal also in difficult optical conditions [20–22]. This contribution proposes a new approach to self-mixing interferometry, based on a high-speed wavelength modulation, for simultaneously retriev-

ing speed and distances information of a non-cooperative target. The high-speed modulation allows to overcome some problems due to speckle patterns, as shown in the next sections. The realized instrument shows an excellent range-resolution trade-off, which is limited only by the laser source characteristics. The instrument performances are compared for three different laser sources. Finally, robustness to speckles is confirmed in industrial environment, working directly on a target wet by running water.

## 2. Self-mixing interferometry

As mentioned, Self-mixing Interferometry is a single channel interferometric technique: the signal is generated by the interference in the laser cavity itself, induced by the light reflected by the target, shifted in frequency by the Doppler effect [2]. When a fraction between  $10^{-4}$  and  $10^{-8}$  of the emitted power is back-reflected, a suitable interferometric signal is measurable. The measured power  $P$  is modulated by  $F(\varphi)$ , which is a periodic function of phase  $\varphi=2ks$ , where  $k=2\pi/\lambda$  is the wave vector,  $s$  is the absolute target distance and  $\lambda$  is the laser diode (LD) wavelength. The interferometric fringes shape varies accordingly to target distance and back-injection variations, as a function of the feedback-parameter  $C$  [3,4]. Briefly, the more distance and the back-reflected fraction increase, the more signal assumes a sawtooth shape. By time differentiation of the interferometric phase, the following equation is obtained:

$$\frac{\partial \varphi}{\partial t} = -2 \frac{2\pi}{\lambda^2} \cdot s \cdot \frac{\partial \lambda}{\partial t} + 2 \frac{2\pi}{\lambda} \cdot \frac{\partial s}{\partial t} \quad (1)$$

According to (1), it is possible to induce an interferometric signal by changing the LD wavelength, even if the target is at rest. In that

*Article history:*

Received 18 April 2016

Received in revised form 6 September 2016

Accepted 11 October 2016 Available online xxx

\* Corresponding author.

Email address: [michele.norgia@polimi.it](mailto:michele.norgia@polimi.it), <http://home.deib.polimi.it/norgia/> (M. Norgia)

case, distance measurement can be carried out by evaluating the signal frequency [14]; indeed, under the hypothesis that the wavelength modulation  $\partial\lambda/\partial t$  is known, and  $\partial s/\partial t=0$ ,  $s$  is proportional to the fringes frequency  $f_{mod}=(\partial\varphi/\partial t)/2\pi$ , induced by the modulation:

$$s = \frac{\lambda^2}{2\frac{\partial\lambda}{\partial t}} \cdot f_{mod} \quad (2)$$

Target movement changes the fringe frequency as well; this contribution  $f_{vel}$  is expressed as:

$$\frac{\delta\varphi_{vel}}{\delta t} = 2\pi f_{vel} \quad (3)$$

The total phase variation is generated by the sum of the two contributions, but it is possible to measure them independently, as described below.

### 3. Measurement method

The aim of this work is the development of a contactless measurement instrument able to simultaneously estimate velocity and absolute distance information. According to this, an efficient way to evaluate separately the two phase contributions shown before is necessary.

Firstly, wavelength variations are obtained by LD current modulation: a triangular wave was selected in order to periodically increase and decrease  $\lambda$ , with amplitude  $\Delta I$  and period  $2T$ . Distance measurement can be performed as described in (2) by evaluating fringes frequency of rising edge and falling edge, respectively defined as  $f_{tone+}$  and  $f_{tone-}$ . When the target is not moving the two frequencies are equal, while in general condition they are given by (4) and (5):

$$f_{tone+} = \left| \frac{1}{2\pi} \frac{\partial\varphi}{\partial t} \right| = \left| -\frac{2s}{\lambda^2} \frac{\partial\lambda}{\partial t} + \frac{2}{\lambda} \frac{\partial s}{\partial t} \right| = \left| -\frac{2sh}{\lambda^2} \frac{\Delta I}{\Delta T} + \frac{2}{\lambda} v \right| \quad (4)$$

$$f_{tone-} = \left| \frac{1}{2\pi} \frac{\partial\varphi}{\partial t} \right| = \left| \frac{2s}{\lambda^2} \frac{\partial\lambda}{\partial t} + \frac{2}{\lambda} \frac{\partial s}{\partial t} \right| = \left| \frac{2sh}{\lambda^2} \frac{\Delta I}{\Delta T} + \frac{2}{\lambda} v \right| \quad (5)$$

Where  $v$  is the target speed and  $h = \Delta\lambda/\Delta I$  is the wavelength modulation efficiency [20]. It is possible to obtain the absolute distance  $s$  as the average of the two frequencies, also canceling the target movement effect:

$$s = (f_{tone+} + f_{tone-}) \left[ \frac{\lambda^2}{2h \left( \frac{\Delta I}{\Delta T} \right)} \right] \quad (6)$$

In the same measurement, the speed information is retrieved with sign, by subtracting the modulation contribution as follow:

$$v = \frac{f_{tone+} - f_{tone-}}{2} \left[ \frac{\lambda}{2} \right] \quad (7)$$

In conclusion, both measurements of absolute distance and speed can be estimated by gated frequency measurements, within a modulation period equal to  $2T$ .

For optimizing the measurement performances, the modulation period should be as short as possible. The advantages of a high-frequency modulation are essentially three: robustness against target movement; robustness against speckle effect and loss of signal; more measurements per seconds and possibility of averages while also discarding unreliable measurements. The first advantage derives directly from the measurement principle: if the modulation frequency is much higher than the bandwidth of the target movements, the measurement is in stationary conditions; in this case, the fringes frequency is almost constant and its value is determined with good accuracy. The robustness against speckle effect increases with modulation frequency, because when the target moves (also transversally) the speckle condition changes rapidly: with a given percentage of available measurements, depending on the focusing condition and the target surface, at a higher modulation frequency, the number of available measurements per second is also higher. If the measurement rate is quite higher than the target movement frequency, we can reconstruct the target speed and distance without loss of information. In addition, resolution can be enhanced by  $\sqrt{N}$  factor when distance is averaged out from  $N$  acquisitions.

The upper limit for the modulation frequency is given by the frequency response of the laser, in terms of  $\Delta\lambda/\Delta I$  [23]. Fig. 1 shows the measured  $\Delta\lambda/\Delta I$  Bode Diagram, obtained by sweeping the frequency range and counting the output fringes number. The laser tested is a Fabry-Perot model, in the near infrared (model HL7851G). For high frequencies, it shows a behavior well fitted by a single pole model (shown in figure). The pole frequency is about 120 kHz.

Given this frequency response, our choice for the modulation frequency was 40 kHz. The measurements in the frequency domain, shown in Fig. 1, were confirmed by the measurements in the time domain: Fig. 2 shows the fringes period measured during the ascend phase of a single triangular modulation with target not moving, compared with the theoretical time response given by a single pole at 120 kHz.

The equivalent single pole frequency  $f_p$  retrieved has been used to pre-emphasize the modulation wave and correct non-linearity. The modulation signal, according to this, becomes a distorted triangular signal wave. Fig. 3 shows the same measurement of Fig. 2, repeated

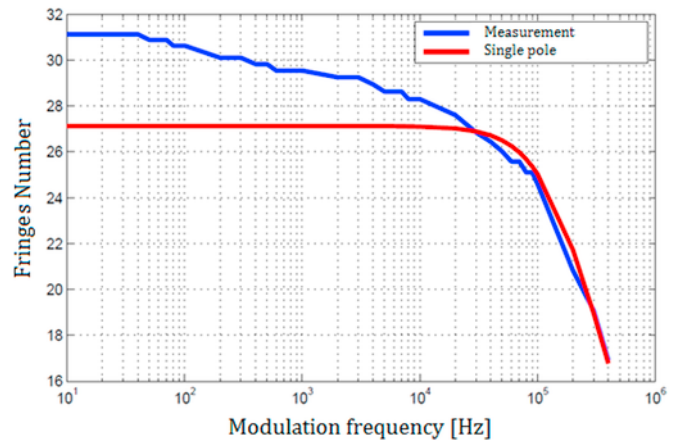


Fig. 1. Wavelength modulation efficiency  $\Delta\lambda/\Delta I$  Bode Diagram, compared with a single pole transfer function.

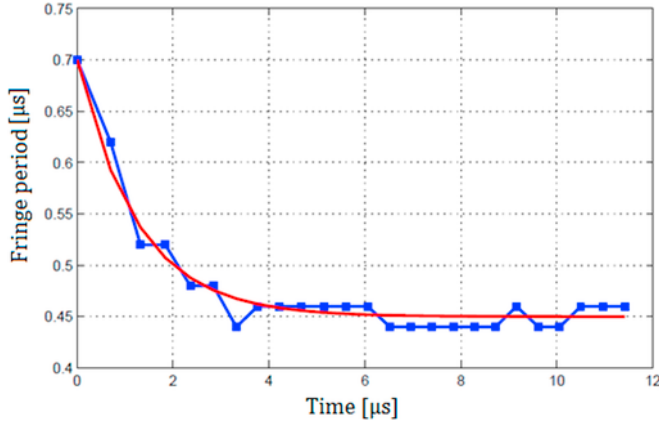


Fig. 2. Fringes period measured during a modulation semi-period (square dots), and single-pole fitting (thick line).

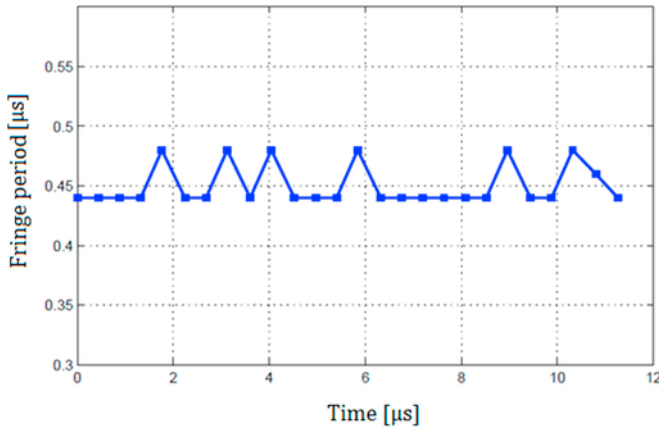


Fig. 3. Fringes period measured during a modulation semi-period, after pre-emphasis of the triangular LD current modulation.

after the pre-distortion of the triangular wave. As expected, the fringes period in this case is almost constant.

In our experiments, the LD current modulation  $\Delta I$  is quite small; therefore, the nonlinearity in  $\Delta\lambda/\Delta I$  is negligible [24]. The proposed instrument is indeed design for a target distance around 1 m, and there is no need for a deep current modulation to achieve a suitable number of fringes: the minimum number of fringes sets the required modulation amplitude necessary to carry out the measurement. The single tone extraction algorithm, through interpolated FFT, works at its best when the signal frequency is at least 5% of the sample frequency  $f_s$  [25]. In that case, a minimum  $\Delta\lambda$  is required to produce enough fringes, which means a minimum modulation current amplitude. This value depends mainly on the desired instrument dynamic range: fringes frequency grows linearly with the target distance, so, if the amplitude is too small, not enough fringes are produced at short distances. On the other hand, the fringes shrink when the target is far and, if  $\Delta I$  is too high, large bandwidth and fast sampling are required. These two conditions set the distance measurement range.

#### 4. Laser sources characterization

The proposed method was tested with three different laser sources: model HL7851G (Fabry-Perot laser at 780 nm), model WSLD-1550 (DFB laser at 1550 nm) and model ML1210 (DFB laser at 1310 nm). Considerations exposed are valid for all of them; how-

ever, a specific  $\Delta\lambda/\Delta I$  characteristic identification is required for each single source.

The proper definition of the modulation amplitude allows to reach the best tradeoff between dynamic and laser non-linearity. As shown in Table 1, HL7851G and WSLD-1550 work at similar polarization current  $I_{pol}$ , as a consequence the selected modulation amplitude  $I_{mod}$  is almost the same. However, the two sources show different sensitivity and singularities: with maximum modulation amplitude, the WSLD-1550 exhibits higher number of fringes than HL7851-G, but a slower response (the pole frequency is around 50 kHz). These features make the WSLD-1550 eligible for short distance measurements despite longer wavelength and nonlinearity. Thus, accurate pre-emphasis is required. On the other hand, HL7851-G has a good linearity and it is suitable for long distances.

ML1210F allows obtaining good sensitivity even with limited  $I_{mod}$  and narrow current range. This laser, though, shows fringes amplitude difference between rising edge and falling edge of modulation wave. This happens, also, to WSLD-1550 signal when  $C$  value increases.

$\Delta\lambda/\Delta I$  varies, also, as a non-linear function of  $I_{pol}$ . They also have completely different trend: Fig. 4 reports  $\Delta\lambda/\Delta I$  for the three laser models.

All the lasers were modulated at the same frequency (40 kHz) and custom pre-emphasis has been designed. Fig. 5 shows the interferometric signal comparison, before and after the pre-emphasis for WSLD-1550: improvement of fringes periodicity is evident, especially at the beginning of the semi-period, close to the triangular wave peak. These signals are obtained after subtraction of the triangular wave amplitude modulation and high-pass filtering.

#### 5. Hardware setup

The instrument design is composed by four parts, and each part is subdivided in blocks as shown in Fig. 6. The main parts are: the optic, the analog circuit, the digital circuit, and the PC (or microcontroller) acquisition and elaboration. The optical system is extremely simple: the laser package contains the photodiode used for monitoring power and a collimator lens sets the focus position. The focusing was manually changed to obtain the desired  $C$  level, however auto-focus can be applied to the system [8,15]. The analog system sets the laser working point, produces current modulation, reads the photodiode current signal and filters it before the analog-to-digital conversion. The analog project is describe in details below.

The laser driver circuit is based upon two operational amplifiers (MCP6021, bandwidth=10 MHz) which respectively set the laser current and the current modulation. The digital circuit provides a 40 kHz square wave; a Miller-integrator amplifier generates the triangular wave and pre-emphasizes the modulation. It introduces a zero to cancel the thermal pole discussed in the previous paragraphs. A final 1 MHz low-pass filter limits the high frequency noise. Driver UCC27424 isolates digital and analog system and regenerates signal edges. A 1 k $\Omega$  resistor, between the digital output and UCC27424 input, limits digital output current and guarantees sharp edges.

Table 1  
Laser sources features.

Source	$I_{pol}$ (mA)	$I_{mod}$ (mA <sub>pp</sub> )	Series resistance ( $\Omega$ )	$f_{pole}$ (kHz)	Sensitivity (cm/MHz)
HL7851G	70	10	25	127	25
ML1210F	32	5	3,75	78	25
WSLD-1550	60	10	1,9	50	60

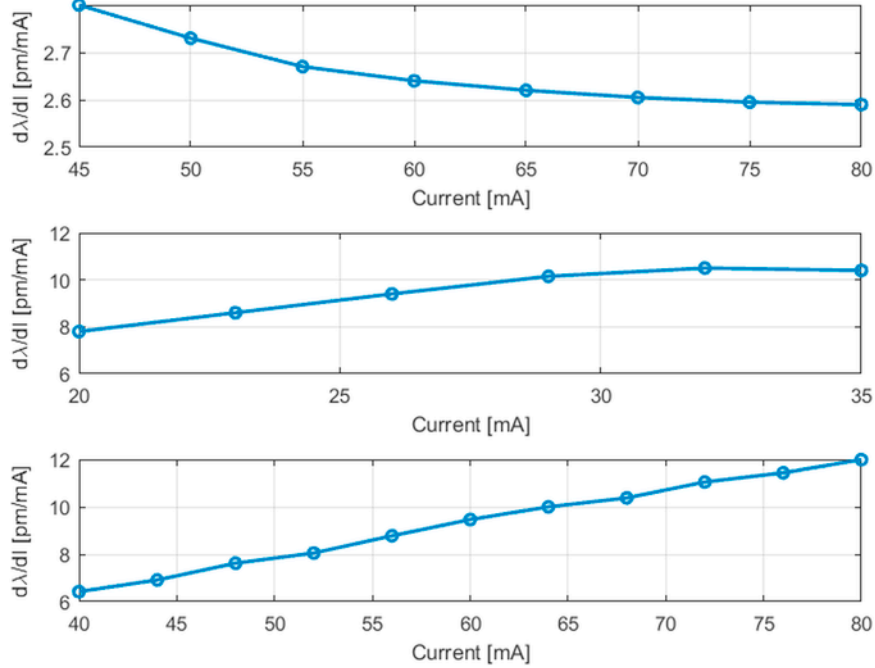


Fig. 4.  $\Delta\lambda/\Delta I$  as function of  $I_{pol}$ . Upper box HL7851-G; center box ML1210F; lower box WSLD-1550.

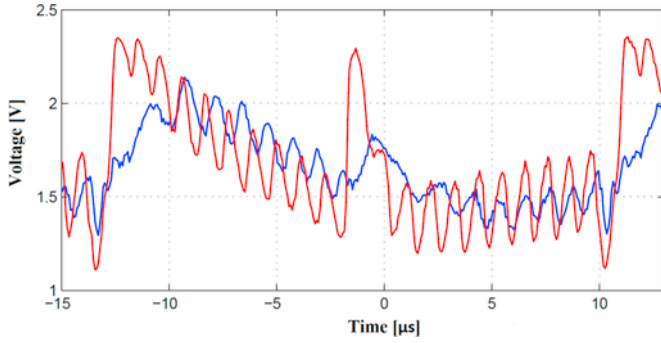


Fig. 5. Interferometric signals before (blue) and after (red) pre-emphasis. (For interpretation of the references to color in this figure legend, the reader is referred to the web version of this article.)

The second analog circuit part reads the photodiode signal and subtracts the modulation contribution due to the laser slope-efficiency. A current buffer uncouples the photodiode capacitance  $C_D$  and a current mirror amplifies it with a gain equal to about 100. Then, a transimpedance amplifier (OPA355, bandwidth 200 MHz) converts current signal into voltage output, and subtracts the modulation wave due to direct power modulation.

The circuit structure is the same for all the tested LDs, despite the modifications required to change  $I_{pol}$  and lasers pinout. The final circuit bandwidth is 10 MHz for the model HL7851-G; 15 MHz for WSLD-1550 and ML1210F (the improvement is due to the lower capacitance of their monitor photodiodes).

The ADC model is THS1230, 12-Bit Resolution, 30 MSPS, with a differential input configuration. The single-ended signal is converted in double-ended for minimizing the disturbances due to the digital circuitry. The conversion stage, based on the differential amplifier LMH6550, produces a differential signal and, in addition, subtracts a small square wave, to completely delete the direct power modulation (the square wave modulation is due to a non-perfect delay matching

between the current modulating and the measured triangular waves). Finally, anti-aliasing passive filter cuts off the signal at 6 MHz.

## 6. Signal processing

Real time signal processing performs both single tone extraction and data control. Firstly, interpolated FFT algorithm [25] executes fringes main-tone analysis, and then digital filters discard useless measurements. Finally, distance and velocity are retrieved as explained in previous paragraphs.

CICLONE IV FPGA acquires analog signal through the ADC model THS1230: the FFT algorithm elaborates 128 samples window with  $f_s = 12,5$  MHz or, alternatively, 256 samples windows with  $f_s = 2$  MHz (removing the anti-alias filter at 6 MHz).

Also with interpolated FFT [25], a higher  $f_s$  produces better frequency estimation, due to the higher samples number, but the requirement on the minimum fringes frequency is still about 5% of  $f_s$ .

The acquisition is synchronized with the modulation triangular wave, generated by the FPGA itself. The gated acquisition eliminates the triangular wave initial transitions (see Fig. 5). Hanning window is applied and FFT IP-core calculates the fringes power spectrum. Then, main tone is extracted and interpolation is executed to obtain fine frequency  $f_{fine}$ . The interpolation algorithm is based on (8):

$$v f_{fine} = (i \mp \delta) f_s \delta = \frac{2\alpha - 1}{\alpha + 1} \alpha = \frac{|X_H(i \mp 1)|}{|X_H(i)|} \quad (8)$$

Where  $i$  is the main-tone bin number,  $|X_H(i)|$  is the main-tone absolute value,  $|X_H(i \mp 1)|$  is the highest absolute amplitude of the two near bins,  $\delta$  is the fractional part obtained by the interpolation.

At this point, FPGA transmits data to a second device. Two prototypes were realized: in the first one, a PC executes data filtering and distance/velocity estimation, with rate of 3 consecutive measurements

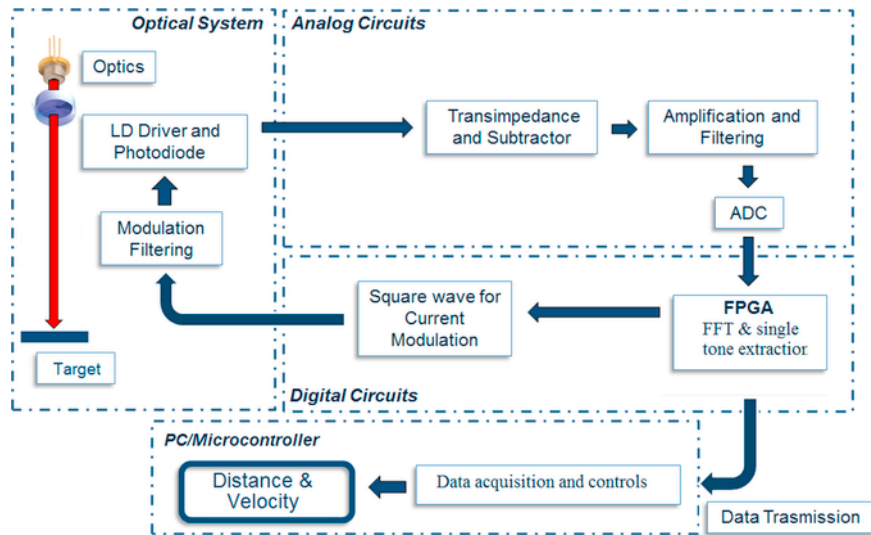


Fig. 6. Instrument block scheme.

transmitted every 2 ms (the rate of 500 Hz is mainly limited by the USB data transmission between FPGA and PC). In the second one, a Micro-controller reads data through SPI and executes data validation control. This solution guarantees measurement frequency of 3 kHz. FPGA transmits main-tone frequency and  $i$ ,  $i+1$ ,  $i-1$  bins amplitudes.

In order to avoid wrong measurements, four controls are implemented:

- Control on the frequency range: spurious reflections or disturbances can generate low or high frequency tone. The algorithm searches the peak in the spectrum only in the range of interest.
- Control on the amplitude: the measurement accuracy is guaranteed when the main tone amplitude is 10 dB higher than noise level. When the measurement does not satisfy this condition, it is discarded.
- Control on standard deviation: algorithm extracts standard deviation of 3 consecutive measurements at 40 kHz. If it shows a realistic value, average and distance/velocity estimation are executed. If not, the data is discarded.

Fig. 7 reports a comparison between the measurement acquisitions with two different data filtering applied on distance measurement. The graphs indicate the valid measurements obtained during time: low-control filter has frequency deviation control set to 10 kHz, applied on three acquisitions, while for the high-control it is set to 2 kHz. The system worked on a black target (with low reflectivity) at about 1 m of distance, and executed 2268 measurements: 68,4% of them are valid with low-control filter, whereas only 6,87% are valid with high-control filter. The accuracy improvement for the high-control is evident, both in distance measurement and in instantaneous standard deviation. It is worthy to note that the applied control operates only on the acquired data, there is no filtering looking at the “expected” values. The remarkable results is that the filtering on the local standard deviation (3 consecutive measurements at 40 kHz), also improves the repeatability of the absolute distance measurement, and the global accuracy, as shown in Fig. 7.

Absolute distance and velocity accuracy depends also on  $\lambda$  stability. DFB lasers WSLD-1550 and ML1210F have a stable wavelength once stabilized in temperature, while HL7851G is a Fabry-Perot laser: its wavelength depends on temperature in a non-deterministic way (it depends on the switch-on procedure, the temperature history

and the aging). Calibration is required to guarantee measurement accuracy. Also, instrument zero adjustment is necessary to compensate for systematic error in velocity calculation, due to a small difference (around 2%) between rising and falling edge frequency.

## 7. Experimental results

An experimental measurement campaign was conducted to characterize the instrument performances and compare the three laser sources. The instrument shows a relative standard deviation (STD) in the order of  $4 \cdot 10^{-4}$  for distance measurements between 15 cm and 2 m. Also for speed measurement, the relative STD is quite good, in the order of  $5 \cdot 10^{-3}$ . Fig. 8 shows the STD of some distance measurements, obtained with HL7851G, acquired on a white paper target, with fixed focus position at 50 cm. These results are obtained for a measurement-time of 25  $\mu$ s, without averaging. As expected, the best result happens in correspondence to the focus position.

Also for speed measurements, the best optical condition is obtained when laser beam is focused just after the target. However, instrument keeps good performances also before the laser focus. Velocity measurement STD is shown in Fig. 9. The target is a rotating disk placed at 50 cm from the laser, with an angle of incidence  $\beta=15^\circ$ . In this case, the speckle effect is evident, because the target surface moves transversally with respect to the laser beam. STD increases with target rotation speed: the instrument shows a relative STD of about  $5 \cdot 10^{-3}$  until 2 m/s. Distance acquisitions on the rotating disk shows that the target movement slightly affects distance measurement precision: in this case the measured relative STD degrades to about  $10^{-3}$ .

Comparison between 128 and 256 samples FFTs is proposed in Table 2: the higher sampling frequency improves the presence of valid measurements.

As previously explained, three different prototypes have been realized and tested. The obtained results are comparable for the three laser sources, but with some differences. ML1210F guarantees a slightly higher resolution (measured by STD), but exhibits a lower sensitivity to back-injection, and therefore lower probability of showing available measurements. WSLD-1550 is similar to HL7851-G in terms of sensitivity, but offers the stability of a DFB, and also the

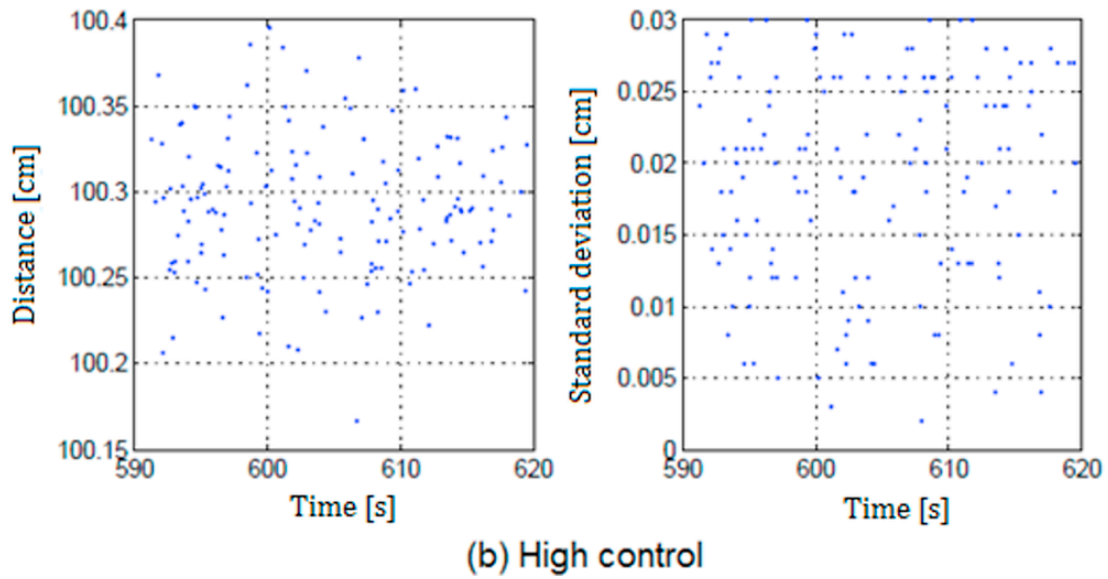
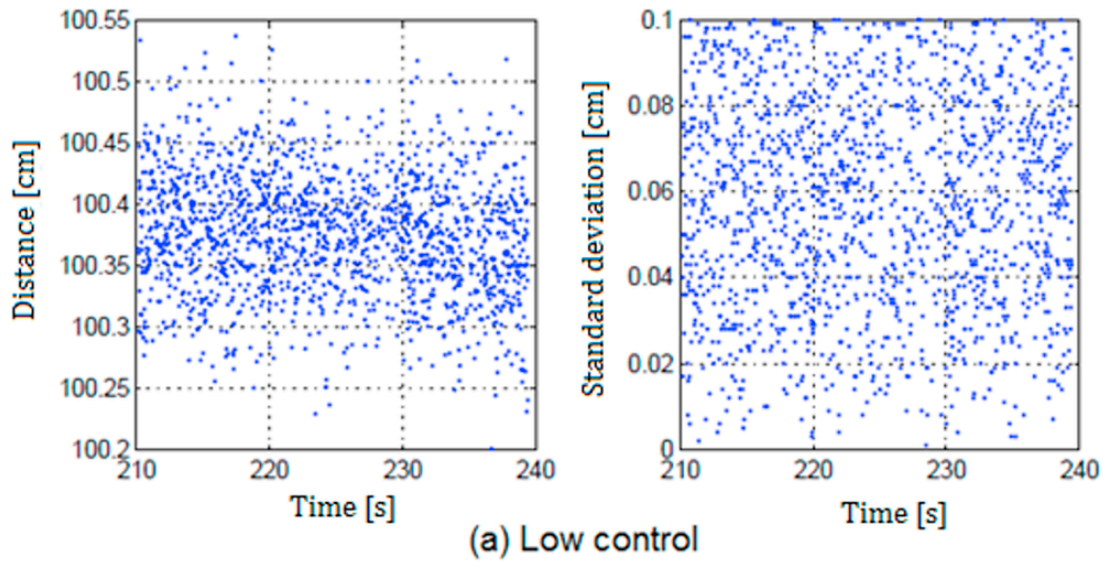


Fig. 7. (a) Low and (b) High control applied to the same measurement distance (100 cm). The left graphs indicate the distance measurement, while the right graphs indicate the standard deviation calculated on 3 consecutive measurements.

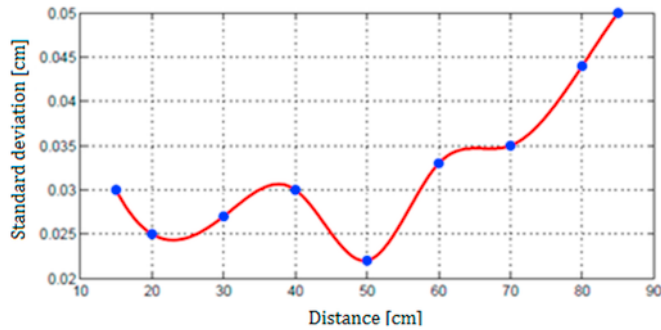


Fig. 8. Distance measurement STD. (focus 50 cm; source HL7851-G).

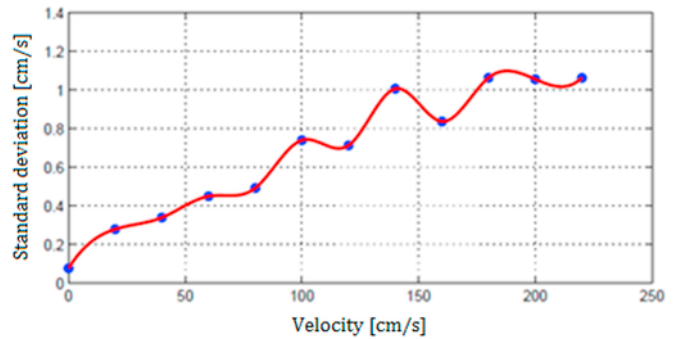


Fig. 9. Velocity measurement STD. (focus 50 cm; source HL7851-G).

**Table 2**  
Comparison between different sampling frequencies.

	$f_{\text{sampling}} = 12,5 \text{ MHz}$		$f_{\text{sampling}} = 25 \text{ MHz}$	
Control	Valid Measurements	% over	Valid Measurements	% over
Low	1592	69,82%	916	80,35%
High	156	6,84%	103	9,03%

possibility to work in safety class I (due to its wavelength), therefore it is the most suitable choice for industrial applications.

For validating the measurement approach and confirming the prototype robustness to speckle incoherence, the realized prototype was tested in an industrial application. Aim of the measurement is tube rotation monitoring during industrial cooling process, realized by a water flow, as shown in Fig. 10.

The target is an opaque iron tube, under a water layer, placed at 90 cm of distance. Laser focus is at 100 cm and incidence angle on the tube is set to  $20^\circ$ . From an optical point of view, this kind of target is one of the worst to be measured: the crude iron surface (black and dirty) does not exhibit a strong reflection by itself, and the amount of water drastically worsen the optical conditions. The first tested source is HL7851G. Results are shown in Fig. 11: at the beginning of the measurement the rotation speed was 55 cm/s; after 10 s it changed to 40 cm/s, and after 250 s the tube was stopped. During the measurement, the amount of water was increased. For the last sec-

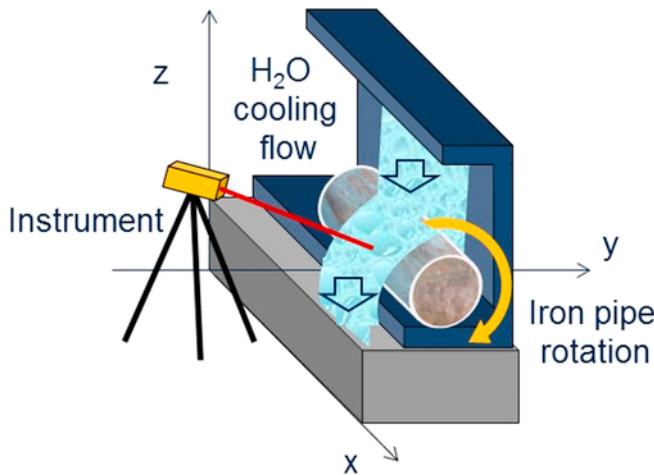


**Fig. 10.** Description of the rotation speed measurement during water cooling flow.

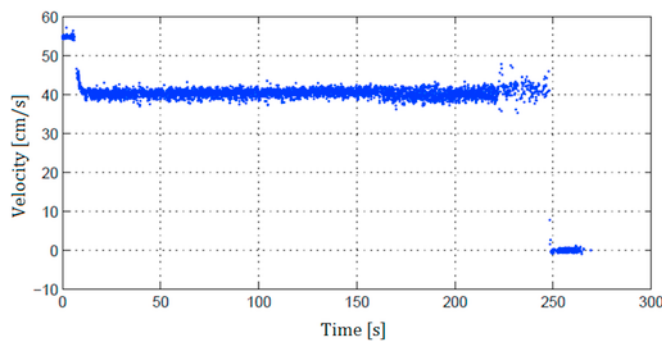


**Fig. 11.** Measurement of the rotation speed of an iron tube during water cooling process.

onds, an additional bottle of water was poured directly on the measurement spot. Until this moment, the local STD was limited to about  $10^{-2}$ . The long-time STD= $5 \cdot 10^{-2}$  is mainly due to the non-uniform tube rotation speed (it is not a limit of the instrument, but a real speed-variation). As expected, the more the water flux increases, the more the number of available measurements decreases. However, measurement reliability is quite constant. The measurement was repeated with laser WSLD-1550, obtaining comparable results.

This extreme test demonstrates the reliability and robustness of the proposed approach: the triangular modulation samples the target motion conditions at high-speed (measurement time limited to  $25 \mu\text{s}$ ), if the signal is not good enough for reliable measurements it is simply discarded. The high speed-rate typically allows keeping a useful number of measurement per second (depending on the mechanical bandwidth under test), even after non-linear filtering and choice of the best measurement data.

## 8. Conclusions

This contribution presents the development of a contactless method for the simultaneous measurement of both distance and velocity, by means of a modulated self-mixing interferometer. Compact and low-cost instrument based on FPGA executes real-time measurements through frequency domain elaboration. A quasi-triangular wave laser current modulation allows producing two interferometric fringes tone for each period; real-time algorithm sums and subtracts the two tones for retrieving distance and velocity information. The 40 kHz modulation frequency allows for a quasi-instantaneous measurement, with respect to typical mechanical frequency response (the measurement time is limited to  $25 \mu\text{s}$ ). Systematic error due to non-linearity has been study and corrected by means of a pre-emphasis. Signal analysis and filtering for data selection were implemented to improve measurement reliability and robustness. The high-frequency acquisition and elaboration guarantees valid measurements even in presence of speckle-pattern and signal loss. In conclusion, experimental measurements demonstrate sensor reliability also in harsh industrial environment, under water flow. Future developments concern the final engineering of the system and the possibility of implementing an auto-focusing system [9,15].

## Acknowledgments

The work was partially supported by Tenaris-Dalmine. The authors wish to thank Dr. Gabriel Solari for the fruitful discussions and collaboration in the industrial measurements.

## References

- [1] S. Donati, Electro-optical instrumentation – sensing and measuring with lasers, Prentice Hall, Upper Saddle River (NJ), 2008.
- [2] E. Baumann, F.R. Giorgetta, J.-D. Deschênes, W.C. Swann, I. Coddington, N.R. Newbury, Comb-calibrated laser ranging for three-dimensional surface profiling with micrometer-level precision at a distance, *Opt Express* 22 (2014) 24914–24928.
- [3] G. Giuliani, M. Norgia, S. Donati, T. Bosch, Laser diode self-mixing technique for sensing applications, *J Opt A: Pure Appl Opt* 4 (2002) S283–S294.
- [4] S. Donati, Developing Self-mixing interferometry for instrumentation and measurements, *Laser Photonics Rev* 6 (2012) 393–417.
- [5] F. Yuanlong, Y. Yu, J. Xi, Q. Guo, Dynamic stability analysis for a Self-mixing interferometry system, *Opt Express* 22 (2014) 29260–29269.
- [6] D. Melchionni, A. Magnani, A. Pesatori, M. Norgia, Development of a design tool for closed-loop digital vibrometer, *Appl Opt* 54 (2015) 9637–9643.
- [7] A. Magnani, D. Melchionni, A. Pesatori, M. Norgia, Self-mixing digital closed-loop vibrometer for high accuracy vibration measurements, *Opt Commun* 365 (2016) 133–139.

- [8] Y.L. Lim, J.R. Tucker, A.D. Rakic, Distance measurement using the change in junction voltage across a laser diode due to the self-mixing effect, *Proc North Opt* (2006) 73–77.
- [9] A. Magnani, A. Pesatori, M. Norgia, Self-mixing vibrometer with real-time digital signal elaboration, *Appl Opt* 51 (2012) 5318–5325.
- [10] T. Taimre, M. Nikolic, K. Bertling, Y.L. Lim, T. Bosch, A. Rakic, Laser feedback interferometry: a tutorial on the self-mixing effect for coherent sensing, *Adv Opt Photonics* 7 (2015) 570–631.
- [11] S. Sudo, Y. Miyasaka, K. Nemoto, K. Kamikariya, K. Otsuka, Detection of small particles in fluid flow using a self-mixing laser, *Opt Express* 15 (2007) 8135–8145.
- [12] Y. Zhao, et al., Self-mixing fiber ring laser velocimeter with orthogonal-beam incident system, *IEEE Photonics J* 6 (2014) 1–11.
- [13] L. Lu, Z. Cao, J. Dai, F. Xu, B. Yu, Self-mixing signal in Er<sup>3+</sup> – Yb<sup>3+</sup> codoped distributed bragg reflector fiber laser for remote sensing applications up to 20 km, *IEEE Photonics Technol Lett* 24 (2012) 392–394.
- [14] A. Magnani, A. Pesatori, M. Norgia, Real-time Self-mixing interferometer for long distances, *IEEE Trans Instrum Meas* 63 (2014) 1804–1809.
- [15] U. Zabit, R. Atashkhoei, T. Bosch, S. Royo, F. Bony, A.D. Rakic, A. D, Adaptive self-mixing vibrometer based on a liquid lens, *Opt Lett* 35 (2010) 1278–1280.
- [16] M. Norgia, A. Magnani, A. Pesatori, High resolution self-mixing laser rangefinder, *Rev Sci Instrum* 83 (2012) 045113.
- [17] Y.L. Lim, R. Kliese, K. Bertling, K. Tanimizu, P.A. Jacobs, A.D. Rakić, Self-mixing flow sensor using a monolithic VCSEL array with parallel readout, *Opt Express* 18 (2010) 11720–11727.
- [18] D. Melchionni, M. Norgia, Optical system for liquid level measurements, *Rev Sci Instrum* 85 (2014) 075113.
- [19] M. Norgia, A. Pesatori, S. Donati, Compact laser-diode instrument for flow-measurement, *IEEE Trans Instrum Meas* 65 (2016) 1478–1483.
- [20] M. Norgia, C. Svelto, Novel measurement method for signal recovery in optical vibrometer, *IEEE Trans Instrum Meas* 57 (2008) 1703–1707.
- [21] Y. Fan, Y. Yu, J. Xi, J.F. Chicharo, Improving the measurement performance for a self-mixing interferometry-based displacement sensing system, *Appl Opt* 50 (2011) 5064–5072.
- [22] A. Magnani, M. Norgia, Spectral analysis for velocity measurement through Self-mixing interferometry, *J Quantum Electron* 49 (2013) 765–769.
- [23] M. Norgia, A. Pesatori, M. Tanelli, M. Lovera, Frequency compensation for a Self-mixing interferometer, *IEEE Trans Instrum Meas* 59 (2010) 1368–1374.
- [24] K. Kou, X. Li, L. Li, H. Xiang, Injected current reshaping in distance measurement by laser self-mixing interferometry, *Appl Opt* 53 (2014) 6280–6286.
- [25] J. Schoukens, R. Pintelon, H. Van hamme, The interpolated fast Fourier transform: a comparative study, *IEEE Trans Instrum Meas* 41 (1992) 226–232.